Concrete in multiaxial compression – a multilevel analysis

J.P.W. Bongers, H.S. Rutten
Eindhoven University of Technology, Faculty of Architecture, Building and Planning, PO Box 513, 5600 MB Eindhoven , The Netherlands

The macroscopic mechanical behaviour of concrete, observed in multiaxial compression tests, is classified according to four typical stages in crack formation. At these stages, the behaviour is analysed at three different scale levels. It appears that most of the observed macroscopic features can be explained by quite simple phenomena when the concrete structure is analysed at the level of aggregate grains embedded in a matrix of cement paste. Based on this analysis, a 2D meso-mechanical model is presented aiming at describing the pre-peak mechanical behaviour of concrete in multiaxial compression tests.

Key words: **Multiaxial compression, numerical modelling, scale levels,** RVE **approach**

1 Introduction

Various phenomena influence the macroscopically observed mechanical behaviour of a normal strength concrete structure loaded in multiaxial compression. For an analysis of these phenomena it is necessary to develop a frame on the basis of which a classification can be made. First of all a distinction is drawn between phenomena taking place at three different scale levels. Secondly, the investigation is divided according to four typical stages in a multiaxial compression test. As the macroscopic mechanical behaviour at each stage is also connected to phenomena on the lower scale levels a frame is created as shown in table 1.

Table 1. Classification of concrete mechanical behaviour.

	Stage 1	Stage 2	Stage 3	Stage 4
Level 1				
Level 2		*Phenomena in concrete mechanical behaviour*		
Level 3				

1.1 *Scale levels*

To link structural features of a heterogeneous material like concrete with phenomena like crack formation, crack propagation and failure, it is convenient to analyse the material on different scale

levels. With this in mind Wittmann (1987) proposed on basis of common practice in material science a practical subdivision into three scale levels:

- Micro level
- Meso level
- Macro level

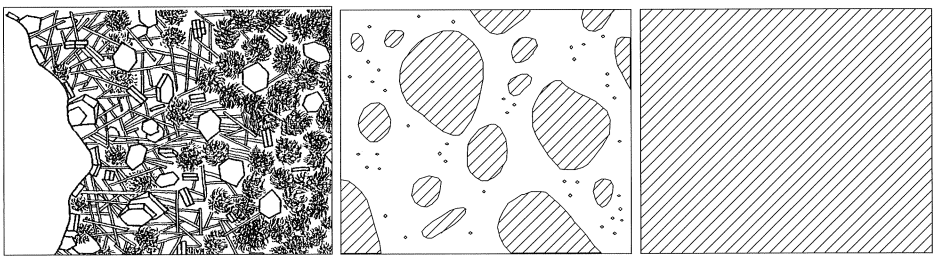

micro level meso level macro level

Fig. 1. Scale levels for concrete.

At the micro level the microstructure and the mechanical properties of the hardened cement paste are considered. The most striking aspect at this level is the existence of an interfacial zone between the aggregate grains and the bulk cement paste in normal strength Portland cement concrete (Larbi 1991). This interfacial zone can be considered as the weakest link in normal strength concrete. The density of pre-existing micro cracks in this zone is higher than in the bulk cement paste and the zone is also the most porous component of concrete. Porosity's up to 50 % have been recorded (Bourdette et al. 1995), the zone occupies 30 to 50 % of the total volume of the cement paste and has a thickness varying from 25 to 100 μm (Larbi 1991).

At the meso level the heterogeneous structure of concrete, a composite of aggregate grains, hardened cement paste, large pores and pre-existing cracks is taken into account. At this level the interfacial zone between the aggregate grains and the bulk cement paste is often schematised as a (weak) interface with zero thickness. Many of the characteristics of concrete mechanical behaviour, observed at the macro level, can be explained by the heterogeneous structure of concrete at this level.

At the macro level concrete is regarded as a homogeneous material. The mechanical behaviour at this level has been described by many – more or less accurate – models, intended for application in structural engineering.

1.2 *Stages in crack formation*

The mechanical behaviour of concrete in multiaxial compression is also classified by dividing a typical multiaxial compression test into four stages. This division is chosen because each of these stages is characterised by its own specific macroscopic mechanical behaviour.

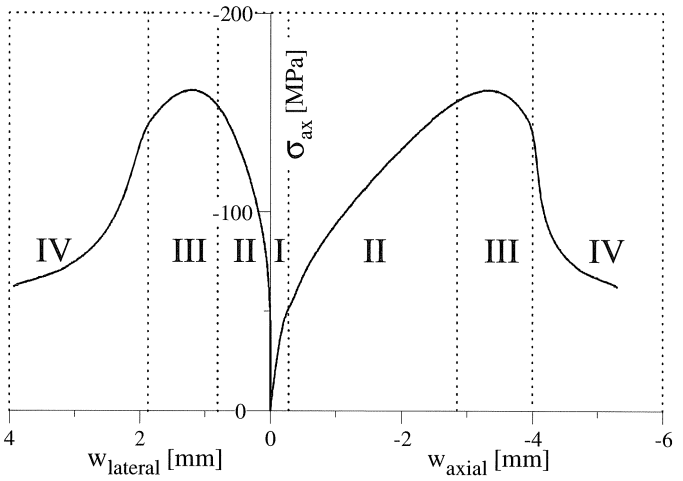

Fig. 2. Stages in a multiaxial compression test.

Figure 2 shows the load-deformation behaviour of a typical multiaxial compression test (plane strain, $\sigma_{lateral}/\sigma_{axial} = -0.15/-1.0$). This test has been part of an extensive test program performed by Van Geel (1995, 1998) at Eindhoven University of Technology. The specific mechanical features of concrete in multiaxial compression at the stages as indicated in figure 2 are discussed in the next sections.

2 Elastic stage (I)

Prior to the application of external loads, a significant number of micro cracks is already present in concrete structures (Slate & Hover 1984). The pre-load cracks are generally bond cracks and are caused by phenomena like drying shrinkage and micro bleeding. Although a lot of pre-load cracks exists, the growth of these cracks and the formation of new bond cracks during initial loading are negligible, thus producing the nearly linear portion of the stress-deformation curve. Consequently, the macroscopic mechanical behaviour at this stage can be described fairly well by applying the classical theory of elasticity.

3 Inelastic hardening stage (II)

The inelastic hardening stage in a multiaxial compression test is characterised by a decrease of the slope in the loading diagram accompanied by inelastic volume compaction. The inelastic volumetric behaviour of the typical multiaxial compression test in figure 2 is displayed in figure 3.

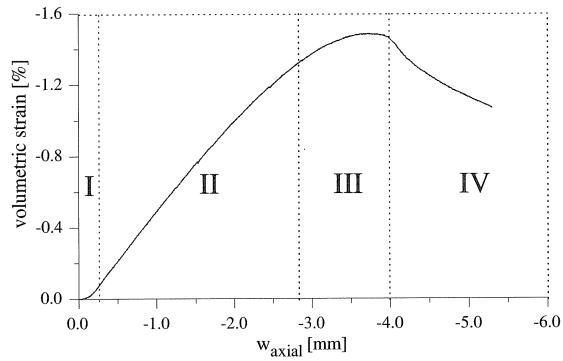

Fig. 3. Inelastic volumetric strain in a multiaxial compression test.

Failure types like tensile and shear failure result in an increase of inelastic volumetric strain. Therefore the displayed volumetric behaviour at stage II must be caused by another phenomenon. When discussing the interfacial bond zone at the micro-level it was stated that the porosity of this zone is very high and considerably higher than the porosity of the surrounding bulk cement paste and aggregate grains. Due to this high porosity crushing failure of the (micro) pore structure of the interfacial bond zone is likely to occur in multiaxial compressive stress states and greatly accounts for the inelastic compactive behaviour in multiaxial compression.

Another characteristic of stage II is that no (macroscopic) cracking occurs that can be seen with the naked eye. At this stage, also no evident damage was visualised by Van Geel (1995) using a vacuum impregnation technique (Goudswaard & Vonk 1989). With this technique internal cracks can be recorded using infrared photography of slices of concrete specimens impregnated with a fluorescent epoxy resin. Using this technique only continuous crack patterns can be visualised, isolated microscopic or mesoscopic cracks remain invisible.

As no continuous cracks could be visualised at stage II, the apparent inelastic behaviour is most probably due to isolated crack formation at the interfacial bond zone. Considering the lateral deformation and the inelastic volumetric (compactive) behaviour this isolated crack formation appears to be a combination of crushing, shear and/or tensile failure.

Crushing failure will only occur in highly porous materials. During crushing the porosity of the bond zone decreases. Once all pores are closed, further crushing of the bond zone will not be possible anymore and an increase of stiffness should be the result. This stiffening effect was already observed by Bazant et al. (1986), by carrying out confined compression tests of small cylindrical specimens loaded up to 2068 MPa. They found indeed that after an initial decrease, the slope of the loading diagram continuously increases.

Postulating that only isolated crack formation at the interfacial bond zone around the aggregate grains occurs, and consequently, that the (macroscopic) strains at stage II are more or less uniformly distributed over the concrete volume, the concrete volume at the meso level can be regarded as a system of springs connected in parallel and in series as shown in figure 4.

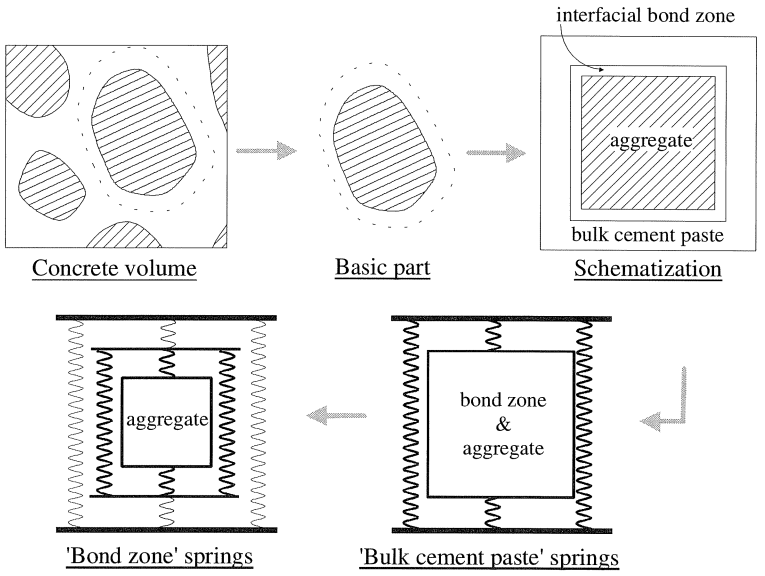

Fig. 4. Schematic "spring" representation of the concrete volume.

At stage II only the stiffness of the "bond zone" springs is reduced. The parallel connected "bulk cement paste" springs keep their initial elastic stiffness. This combination of springs causes a branch with a positive inclination – yet with a considerable decrease in stiffness – in the loading diagram. The spring representation of the concrete volume may also account for the characteristic unloading/reloading behaviour at stage II. Figure 5 shows a cyclic plane strain multiaxial compression test performed by van Mier (1984) at Eindhoven University of Technology.

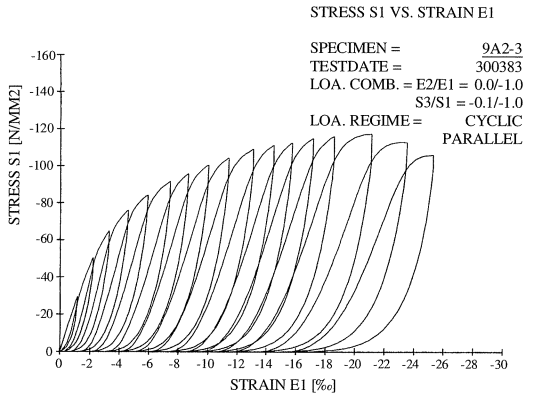

Fig. 5. Cyclic multiaxial compression test (Van Mier 1984).

After an initial steep slope, the unloading curve displays a continuously decreasing slope. According to figure 5 reloading takes place with initial low stiffness, which is gradually increasing until the monotonic curve is almost reached. In this respect it should however be mentioned that figure 5 shows the LVDT measurements. Surface measurements for biaxial cyclic tests (Van Mier 1984) displayed no distinct initial low stiffness at reloading. Although these biaxial tests show very little stage II behaviour, it is suggested that some kind of contact-effect between the specimen and the loading platen may also (partly) account for the initial low stiffness at reloading.
According to the spring representation and supposing there are plastic deformations due to crushing present at the bond zone, unloading of the concrete volume occurs as follows. At first, the stresses in all springs decrease according to initial elastic stiffness until the stresses in the bond zone – and consequently in the, in series connected, aggregate grains – become zero. At this point the stresses in the parallel connected bulk cement paste are not zero because no plastic deformation is present in this component. At further unloading the bond zone opens with no further decrease of stress because no tensile stresses can be transferred across the crushed bond zone. Further decrease of stresses will therefore only occur at the parallel connected bulk cement paste springs, with a considerably less steep unloading branch as a result.
Reloading occurs solely at the parallel connected bulk cement paste springs until the open bond zones are closed again. From then on, reloading of the entire system takes place and initial elastic stiffness is recovered.

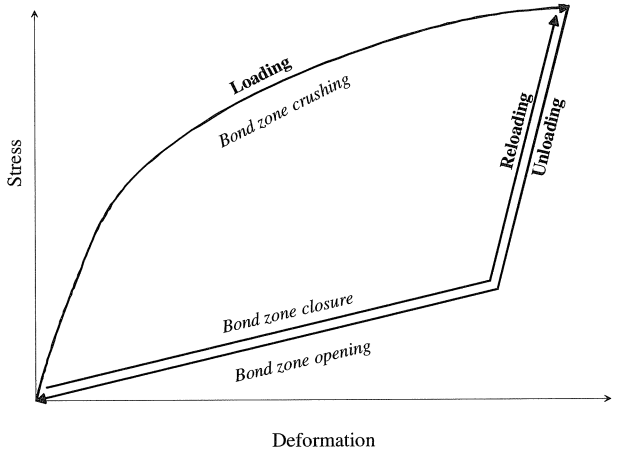

Fig. 6. Load cycle of a basic part of the concrete volume according to the spring representation.

Postulating that bond zone crushing takes place and that the mechanical behaviour at stage II is represented well by the spring mechanism above, an opening at the bond zones (perpendicular to the loading direction) should be present after unloading a specimen previously loaded in multiaxial compression. With this in mind Van Geel et al. (1997) analysed the damage at the interfacial bond zones after unloading from stage II, using microscopic photography. Unlike the vacuum impregna-

tion technique discussed before, this technique enables also isolated cracks to be visualised. These microscopic photographs showed indeed openings at the bond zones perpendicular to the main loading direction up to 50 μm.

4 Around peak stress (III)

At the macro level stage III is characterised by reaching the ultimate strength and the development of macroscopic (shear) cracks. At the meso level crack arrest through the bulk cement paste between the present bond cracks occurs. The formation of macroscopic (shear) cracks produces inelastic increase of the concrete volume. As a consequence, the inelastic volumetric behaviour changes gradually from compaction to dilation (figure 3).
The different crack patterns observed in multiaxial compression tests (highly localised shear bands) and in uniaxial compression tests with little boundary restraint (combined shear and tensile cracks) (Van Mier 1984, Vonk 1992) can be explained at the meso level by the phenomenon of aggregate interlock.
As, for normal strength concrete, the strength of the aggregate grains is much higher than the strength of the surrounding cement paste, crack propagation stops when the cracktip meets an aggregate grain. In this case there are three possible mechanisms for crack propagation (figure 7):

1. Through the aggregate grain
2. Around the aggregate grain (compressive side)
3. Around the aggregate grain (tensile side)

The formation of tensile cracks in concrete requires a very little amount of energy. Hence, mechanism 3 will generally occur. This explains the formation of combined shear/tensile cracks in uniaxial compression.

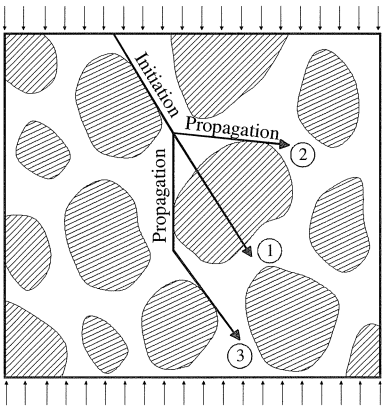

Fig. 7. Mechanisms for crack propagation.

In multiaxial compression crack propagation according to mechanism 3 involves a strengthening mechanism. If the crack is not straight (mechanisms 2 & 3), both the axial and lateral loads will be transferred through the (reduced) contact area of the crack. Figure 8 shows that for mechanism 3 the local crack stresses in *axial* direction are equal to those for mechanism 1. However, the local crack stresses in *lateral* direction are much higher for mechanism 3 than for mechanism 1.

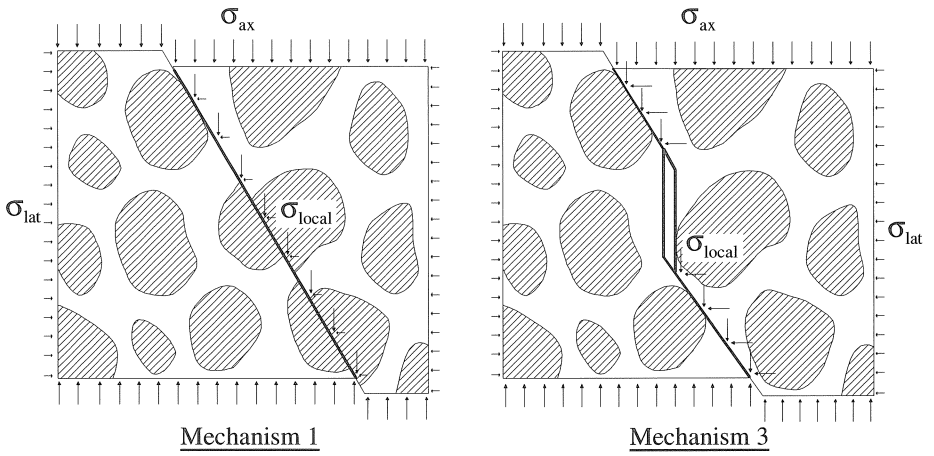

Fig. 8. Local crack stresses in multiaxial compression.

As concrete is a frictional material the local stress state in the contact area of the crack (mechanism 3) is less favourable for crack propagation, so a strengthening mechanism is induced. This strengthening mechanism proceeds until the crack propagates around the "locked" aggregate grain or failure through the aggregate grain occurs.

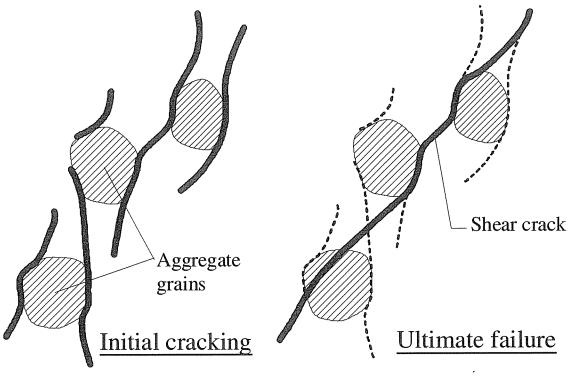

Fig. 9. Crack interface bridging in multiaxial compression (redrawn from Van Mier (1992)).

This cracking mechanism explains the existence of small mesoscopic tensile cracks in macroscopic shear bands in normal strength concrete loaded in multiaxial compression. These arrays of tensile cracks were already reported by Stroeven (1973). In analogy with the formation of crack interface bridges in tension, Van Mier (1992) reported this cracking mechanism as crack interface bridging in compression.

The extent of strengthening due to aggregate interlock, and consequently the influence of a multiaxial compressive stress state, depends on three factors:

- The strength of the aggregate grains related to the strength of the bond zone and the bulk cement paste.
- The size of the aggregate grains.
- The distance between the aggregate grains.

These factors are properties of the concrete mix. However, the distance between the aggregate grains depends not only on the initial situation but may also change during loading. As indicated in figure 10 the contact area of a macroscopic crack is situated at those places where the local crack angle is most perpendicular to the main loading direction. These places correspond to the regions where compressive crushing of the bond zone has occurred at stage II.

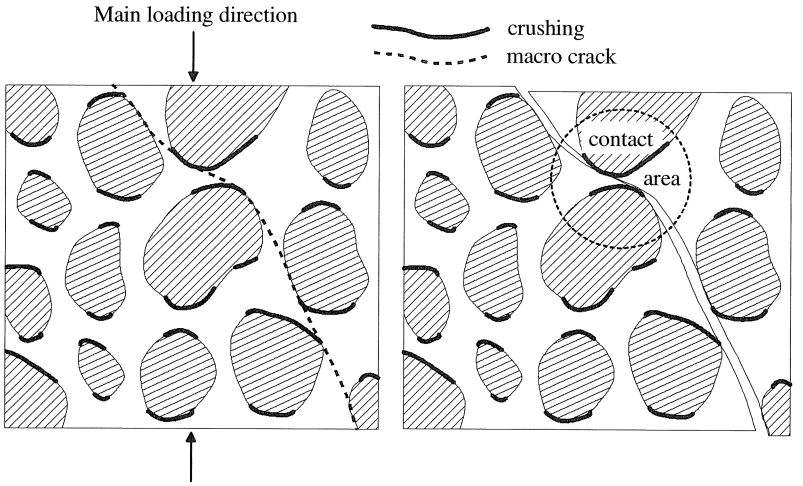

Fig. 10. Contact area of a macroscopic crack and regions of compressive crushing in bond zones.

Accordingly, crushing of the bond zone at stage II decreases the normative distance between the aggregate grains – deformations between the aggregate grains up to 20% may be expected considering the amount of crushing found by Van Geel et al. (1997) – and a higher ultimate strength may be the consequence.

This phenomenon was investigated experimentally by Van Geel (1998). For several proportional plane strain multiaxial compression tests ($\sigma_{lateral} / \sigma_{axial} = -0.05/-1.0$) a preloading was applied by Van Geel. These preloadings did not exceed stage II, so cracking was restricted to the interfacial bond zone. It was postulated that a higher level of preloading would result in more crushing, i.e. in

a shorter distance between the aggregate grains. Figure 11 shows the results of the multiaxial compression tests with and without preloading. It appears that there is indeed a strong correlation between the ultimate strength in multiaxial compression and the amount of crushing.

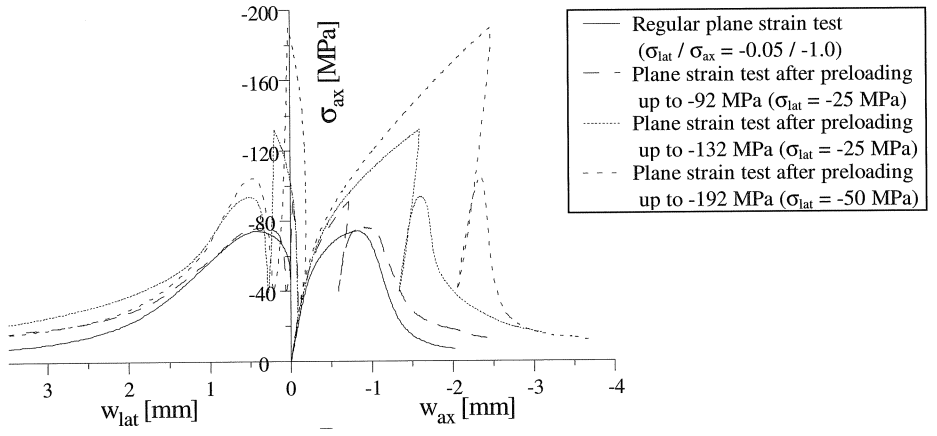

Fig. 11. Ultimate strength in multiaxial compression with / without preloading (Van Geel 1998).

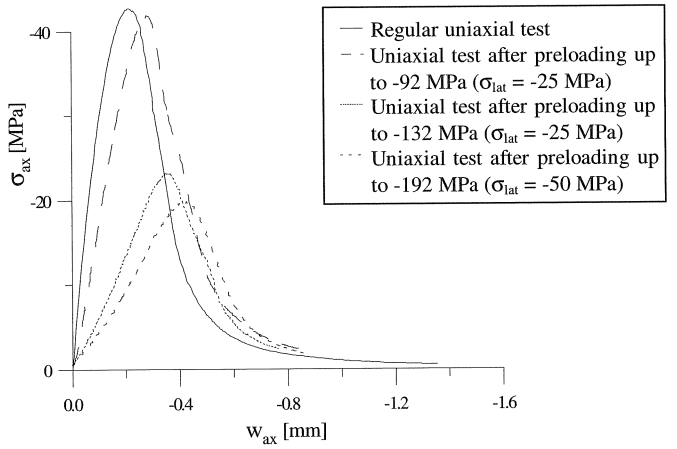

Fig. 12. Ultimate strength in uniaxial compression with / without preloading (Van Geel 1998).

The influence of a multiaxial preloading on the ultimate strength in uniaxial compression was also investigated. These results are displayed in figure 12. It appears that for uniaxial compression the ultimate strength decreases with increasing multiaxial preloading. This is not surprising as the strengthening effect due to aggregate interlock is not present in uniaxial compression. Because of the lack of lateral forces, cracking according to mechanism 3 (figure 7) does not lead to a concentration of lateral loads into the crack contact area. Consequently, crack propagation according to this mechanism can continue without an increase of external loads. It seems therefore that the ultimate strength in uniaxial compression is much more determined by the cohesive strength of the bond zone and the bulk cement paste, rather than by the frictional characteristics. As the average cohesive bond strength decreases at stage II, multiaxial preloading will result in a decrease of the ultimate uniaxial compressive strength.

5 Softening stage (IV)

Stage IV is characterised by a decrease of strength and the propagation of large macroscopic cracks. The mechanical behaviour is determined by increasing deformations in the localised macroscopic cracks, while the continuum in between is unloading. This phenomenon is clearly shown in figure 13. The figure shows a plane strain multiaxial compression test ($\sigma_{lateral}/\sigma_{axial} = -0.05/-1.0$). In this particular test not only the overall stress-deformation behaviour was measured (LVDT's), but also the stress-deformation behaviour of the continuum (strain gauges). By subtracting the average continuum stress-deformation behaviour from the overall stress-deformation behaviour, the average stress-deformation behaviour of the localised macroscopic crack was obtained.

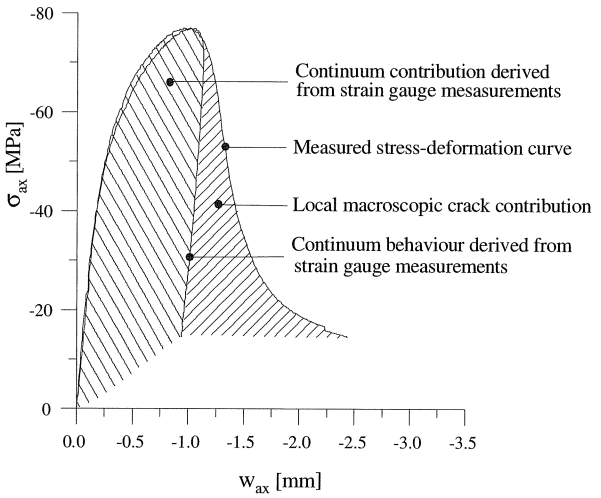

Fig. 13. Continuum versus local behaviour (Van Geel 1998).

It appears that during stage IV the deformations localise in macroscopic cracks. This leads to a strong dependency on the geometry and the boundary conditions of the structure. As a consequence the stress-deformation behaviour at stage IV can not be evaluated apart from the geometry of the specimen and its boundary conditions.
The shape of the descending branch at stage IV also depends strongly on the loading path. Figure 14 shows the loading diagrams of three plane strain compression tests with different loading paths. It appears that the ductility of the softening curve increases when the direction of the stress path becomes more perpendicular to the (schematic) failure surface.
This phenomenon becomes obvious when the ultimate failure surface - after loss of cohesion and/or friction - is considered. A loading path perpendicular to the failure surface results only in a small stress drop after reaching peak strength, while a proportional loading path leads to a very large stress drop beyond the peak.
The reduction of load bearing capacity of the macroscopic crack at stage IV may be caused by two phenomena:

1. Loss of cohesive strength, i.e. failure of crack interface bridges.
2. Decreasing frictional characteristics.

The first cause results in very brittle behaviour and produces the brittle softening curve in tensile tests. The softening curve in multiaxial compression tests is however much more ductile. It seems therefore that the shape of the softening curve in these tests is mainly the result of decreasing frictional characteristics during shearing. The loss of cohesive strength occurs mostly during crack formation and propagation at stage II and III, discussed in the previous sections.

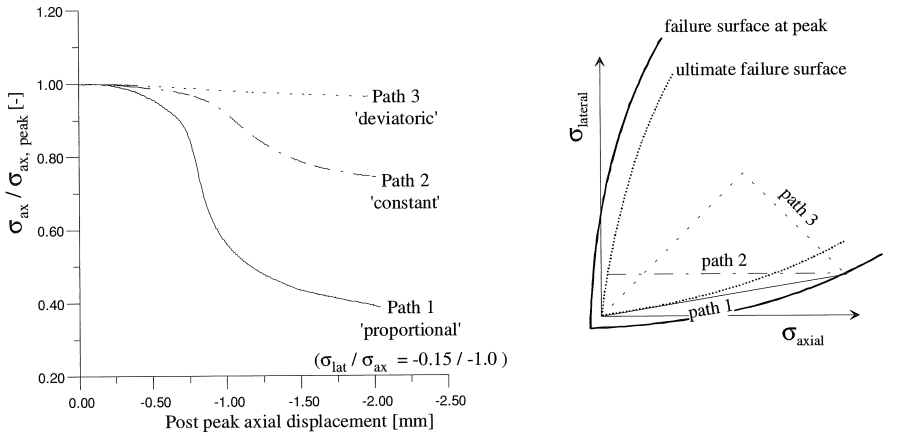

Fig. 14. Post peak curves of multiaxial plane strain compression tests.

6 Numerical modelling in a mesoscopic layout

According to the frame shown in table 1 a classification is made of the most relevant phenomena determining the mechanical behaviour of concrete in multiaxial compression. From the author's point of view a correct description of these phenomena should be the basis of any numerical model aiming at simulating the behaviour of normal strength concrete in multiaxial compression.
As the macroscopic mechanical behaviour observed in multiaxial compression tests could be explained by considering quite simple features of the concrete composite at the meso level, these features should be incorporated. There are two fundamental ways of taking into account the heterogeneous mesostructure of concrete:

- Explicit consideration of the geometrical features of the heterogeneous mesostructure, e.g. by generating mesoscopic meshes in Finite Element computations.
- Implicit consideration of the heterogeneous mesostructure in the macroscopic constitutive (and possibly kinematic) equations.

Although the first method is physically the most appealing method, the impact on computational capacity and time is considerable. To reduce the computational effort to an acceptable extent, a method is pursued with both explicit and implicit consideration of the mesostructure of concrete.

6.1 *Limitations of the present formulation of the model*

A numerical model has been worked out for simulating the mechanical behaviour of stage I – elastic stage – and stage II – inelastic hardening stage – in a plane strain (2D) configuration. For stages III and IV the numerical modelling is near completion. This part will be reported elsewhere. The model as reported here aims at reproducing the salient macroscopic characteristics of the first two stages in plane strain multiaxial compression tests:

- Initially (nearly) elastic behaviour during stage I
- Considerable decrease of the slope in the loading diagram during stage II
- Inelastic volumetric compaction at stage II
- Typical unloading/reloading behaviour at stage II

6.2 *Mesh generation*

A code has been written for the generation of 2D Finite Element Meshes resembling the mesostructure of concrete. This mesh generation code is adapted from a method used by Vonk (1992) and is extensively described in Bongers (1998). The generation code produces an irregular mesh of coarse – polygon shaped – aggregate grains in a matrix of mortar (see figure 15).

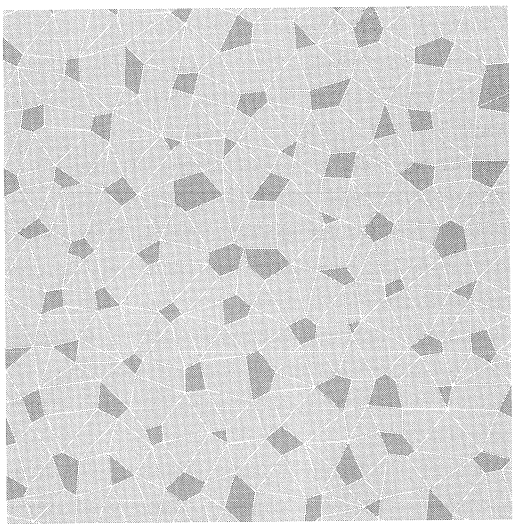

Fig. 15. Generated mesostructure of concrete.

In this way the largest fraction of aggregate grains (5-8 mm.) of the concrete mix used by van Geel (1995, 1998) is explicitly modelled in the Finite Element Mesh. This means that in the present model, the heterogeneous mesostructure of the concrete is reduced to a heterogeneous composite of coarse aggregate grains embedded in a homogenised matrix of small aggregate grains, bulk cement paste and bond zone. For the homogenised matrix of small aggregate grains, bulk cement paste and bond zone, the heterogeneous mesostructure is taken into account implicitly in macroscopic constitutive equations.

6.3 *The concept of a Representative Volume Element* (RVE)

The averaging method used to establish the homogenisation of the heterogeneous mesostructure of small aggregate grains, bulk cement paste and bond zone, is based on the concept of a Representative Volume Element (RVE). The term RVE was first put forward by Hill (1963). For a heterogeneous mesostructure, an RVE for a material point of a continuum mass is a material volume that is statistically representative for the infinitesimal material neighbourhood of that material point. To be representative the RVE should, for randomly ordered mesostructures, include a very large number mesoheterogeneities. If the material has a periodic mesostructure, the RVE can be reduced to one unit cell.

In recent years, the RVE approach has among others been used by Chang (1993) for granular materials, by Onck (1997) for polycrystalline metals and by Smit (1998) for heterogeneous polymers. They used either an RVE of many mesoheterogeneities (Chang) or a unit cell for – assumed – periodic microstructures (Onck, Smit). In all cases the boundary conditions of the macroscopic element are applied to the RVE. Subsequently, using usually the Finite Element Method, the response of the RVE is calculated. This response is assumed to be representative for the whole macroscopic element. In this way, a considerable gain in computer time is accomplished compared to Finite Element computations of the entire meso- or microstructure.

Although the main objective of the RVE-approach is to gain computer time, the accuracy of the method should also be considered very well. In this respect, the optimum choice of an RVE would be one that includes the most dominant features having first-order influence on the overall properties of interest and, at the same time, yields the simplest model. The most dominant mechanical features of concrete in multiaxial compression at stage I and II have been expounded in sections 1.2 and 1.3. It has also been shown that consideration of the basic part as displayed in figure 4 can account for these dominant features. Taking this basic part as an RVE in the form of a unit cell seems therefore an appropriate choice.

6.4 *Effective elastic moduli of the* RVE

Applying the exact shape of the basic part in figure 4 as an RVE results in a dependency on the coordinate system. Therefore the shape of the RVE is adapted to the circular shape as shown in figure 16.

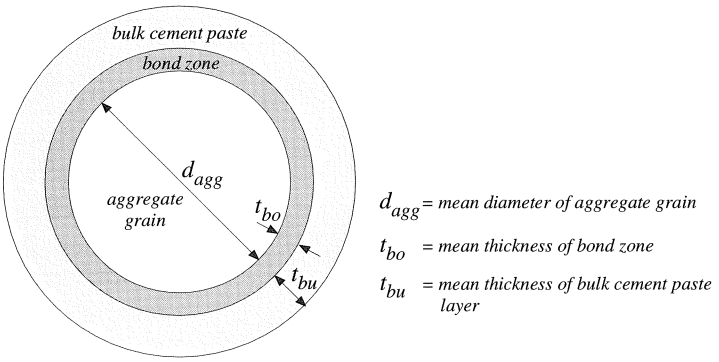

Fig. 16. Choice of an RVE *for normal strength concrete in a 2D configuration.*

Instead of using the Finite Element Method to determine the global elastic behaviour of the RVE, effective elastic moduli of the RVE are calculated analytically. In this way again a considerable gain in computation time is accomplished. The effective elastic moduli of the RVE can be determined by considering both the heterogeneous RVE and an equivalent homogeneous solid with an overall geometry identical to that of the RVE. By applying the same boundary conditions to the heterogeneous RVE as well as the homogeneous solid, and equate the global mechanical response to these boundary conditions, the effective elastic moduli of the RVE can be determined. In this way, two bounds for the effective elastic moduli can be calculated:

1. Applying the same stress boundary conditions to the RVE and the homogeneous solid and equate the resulting mean boundary strains (macrostress prescribed).
2. Applying the same strain boundary conditions to the RVE and the homogeneous solid and equate the resulting mean boundary stress (macrostrain prescribed).

In either case, the effective elastic moduli can be determined from the dimensions and elastic properties of the individual components by considering the two loading cases shown in figure 17. These loading cases have exact analytical solutions. These solutions and their derivation can be found in

Bongers (in prep.). For the RVE considered here, the macrostrain approach and the macrostress approach yield the same solution for the effective elastic moduli. However, important differences in the exact distribution of stresses are present when the macrostress approach is pursued instead of the macrostrain approach.

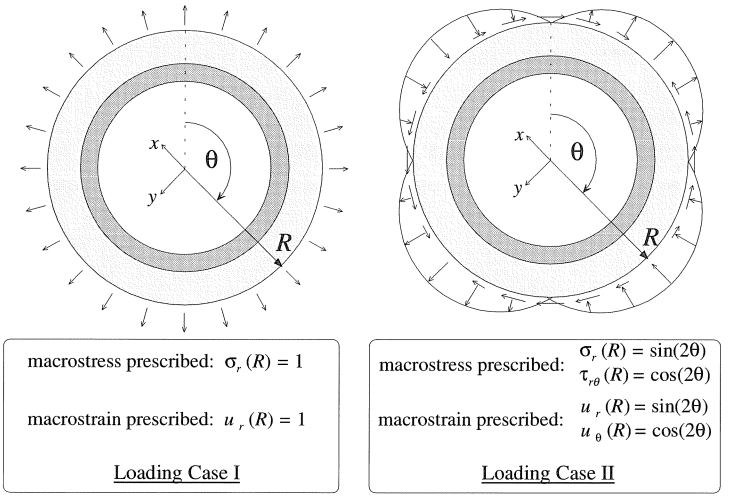

Fig. 17. Loading cases in polar coordinates having exact solutions.

6.5 *Elastic stresses in bond zone*

To compute the elastic stress distribution in the bond zone, either the macrostrain approach or the macrostress approach has to be pursued (or a combination). Although a well-founded choice can not be made a priori, the present model uses the macrostrain prescribed solution. Transformation of the (macrostrain prescribed) loading cases in figure 17 from polar (r,θ) coordinates to rectangular (x,y) coordinates yields for both loading cases a constant macrostrain (ε^{macro}) of:

$$\text{CaseI}: \quad \varepsilon^{macro}(x) = 1, \quad \varepsilon^{macro}(y) = 1$$

$$\text{CaseII}: \quad \varepsilon^{macro}(x) = -1, \quad \varepsilon^{macro}(y) = 1$$

For constant strain elements, any loading case can now be written as a linear combination of these two loading cases. As the exact elastic stress distributions in the bond zones for the two loading cases in figure 17 are known, the elastic stress distribution of an arbitrary loading case can be computed as a linear combination of these two loading cases.

6.6 *Inelastic behaviour (stage II)*

In section 3 it was expounded that the macroscopic observed mechanical features at stage II of concrete in multiaxial compression can be explained by isolated crack formation at the interfacial bond zone, caused by tensile, shear and crushing failure.

The first two types of failure are captured by bounding the stresses in normal (n) and shear (s) direction by a linear Mohr-Coulomb type failure surface (see figure 18), allowing the initiation of an interfacial crack along the direction of the bond zone. The model is formulated according to the classical theory of plasticity with linear cohesive softening. In the compressive region ($\sigma_{nn} < 0$), pure shear failure occurs with no dilatancy. In the tensile region ($\sigma_{nn} > 0$), combined shear/tensile failure occurs depending on the ratio between shear and normal tensile stress (see figure 18).

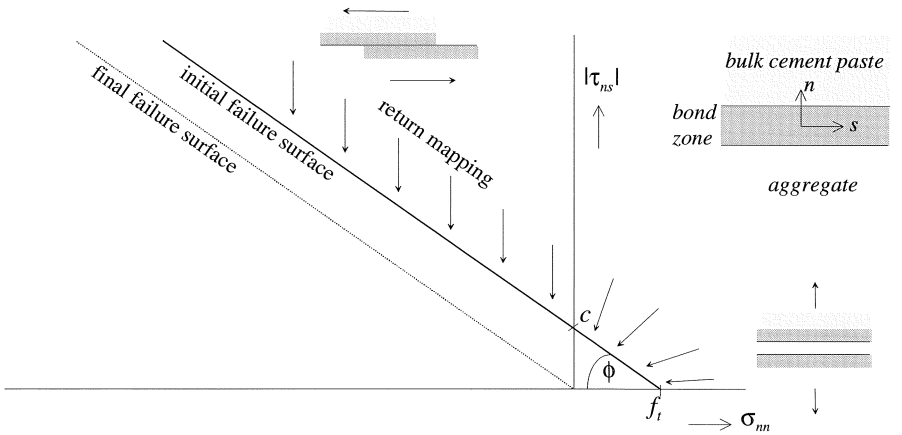

Fig. 18. Shear/tensile failure of bond zone.

Especially during an unloading/reloading cycle in a multiaxial compression test, crack closing phenomena become very important. Capturing this, the present model allows no compressive force transfer between the crack faces if a crack is open. Consequently, no compressive forces will arise during crack closure.

6.7 *Compressive crushing*

Due to the high porosity of the bond zone crushing failure in triaxial compression may also take place. If the stresses – in any direction – within the bond zone are assumed to be bounded by also a straight Mohr-Coulomb type failure surface (characterised by the cohesion (c_{cr}) and the friction angle (ϕ_{cr})), it can be derived that the failure surface with respect to crushing resembles an ellipse in the τ_{nn} - τ_{ns} space (Bongers 1997).

$$f_{\text{crushing}} = |\tau_{ns}| - \sqrt{\sin^2\phi_{cr}\left(\frac{c_{cr}}{\tan\phi_{cr}} - \tau_{ss} - \frac{1}{2}(\tau_{nn} - \tau_{ss})\right)^2 - \frac{1}{4}(\tau_{nn} - \tau_{ss})^2}$$

During compressive crushing the porosity of the bond zone decreases. As the occurrence of crushing is strongly related to the porosity, subsequent crushing will therefore only take place if the load increases. This phenomenon is captured by causing the cohesion (c_{cr}) to grow with decreasing porosity.
Eventually the failure surfaces for shear/tension and crushing are joined together and the overall failure surface of figure 19 is obtained.

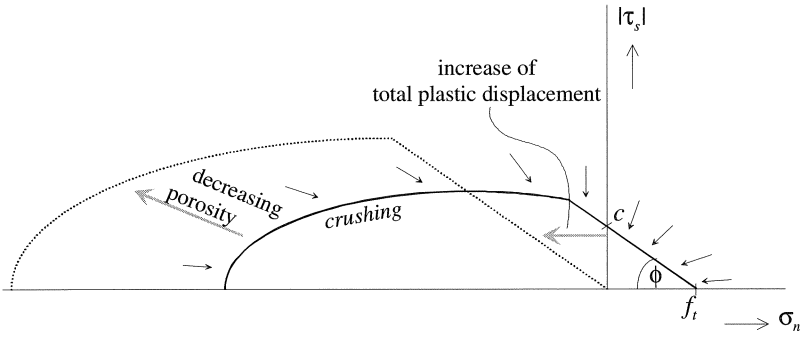

Fig. 19. Movement of combined failure surface.

6.8 *Examples*

The performance of the numerical model is illustrated by simulations of three multiaxial plane strain compression tests performed by Van Geel at Eindhoven University of Technology (Van Geel 1998). These proportional tests, with 5%, 10% and 15% ratio between lateral and axial boundary forces, are performed on cubic specimens of $100 \times 100 \times 100$ mm^2. The test layout is displayed in figure 20. To show the performance of the model in case of a load reversal a simulation of a 10% plane strain compression test is also carried out with a complete unloading/reloading cycle (see figure 22). The simulations are carried out with uniform boundary displacement of the loading platens. To reduce frictional forces at the boundary, the experiments of Van Geel are carried out with teflon layers between loading platens and the specimen. These teflon layers are modelled by adding interface elements with low frictional restraint ($\tan\phi = 0.012$) between the loading platens and the specimen. The computations are carried out with UDEC (Itasca Consulting Group), a computer code based on the Distinct Element Method.

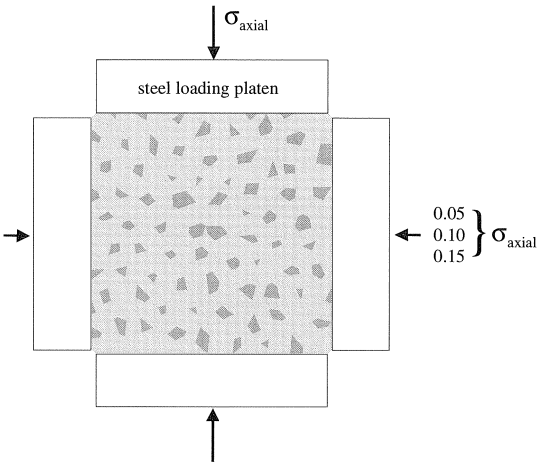

Fig. 20. Test layout for simulations of multiaxial plane strain compression tests.

The input parameters of the model are listed in table 2. The relative areas of aggregate, bond zone and bulk cement paste are based on the properties of the concrete mix used by Van Geel in the experiments (area of bond zone is taken as 40 % of total area of cement paste).

Table 2. Input parameters.

Relative area of aggregate:	70 %
Relative area of bond zone:	12 %
Relative area of bulk cement paste:	18 %
Moduli of Elasticity, Poisson's ratio's:	
E_{agg} = 80000 MPa	
E_{bond} = 7000 MPa	
E_{bulk} = 15000 MPa	
$\nu_{agg} = \nu_{bond} = \nu_{bulk} = 0.07$	
Properties shear/tensile failure mechanism:	
ϕ = 35°	
$f_{t,ini}$ = 4.0 MPa	
Total plastic displacement at which $f_t = 0$ (linear softening): 4.0 μm.	
Properties crushing failure mechanism:	
ϕ_{cr} = 35°	
$c_{cr,ini}$ = 11.2 MPa	(at zero inelastic compaction)
$c_{cr,end}$ = 56 MPa	(at maximum inelastic compaction)
Porosity of bond zone (maximum inelastic compaction): 50 %	

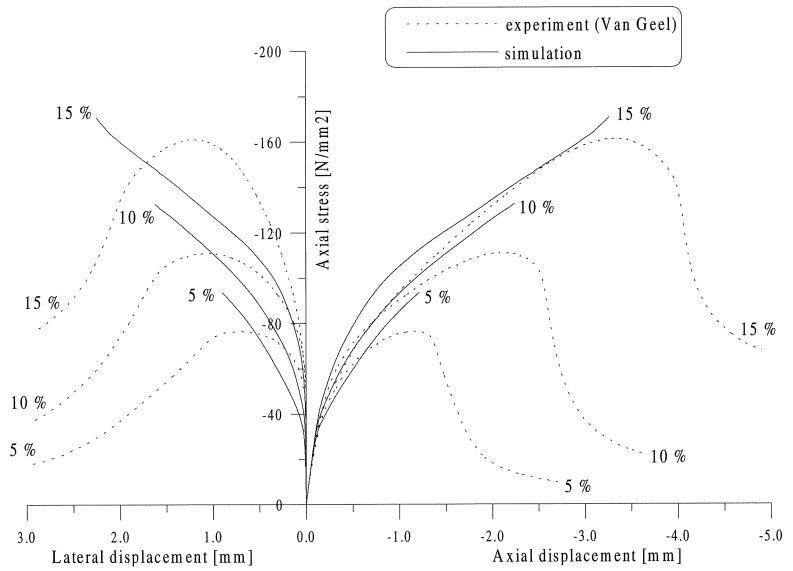

Fig. 21. Results of numerical simulations and comparison with test results (Van Geel 1998).

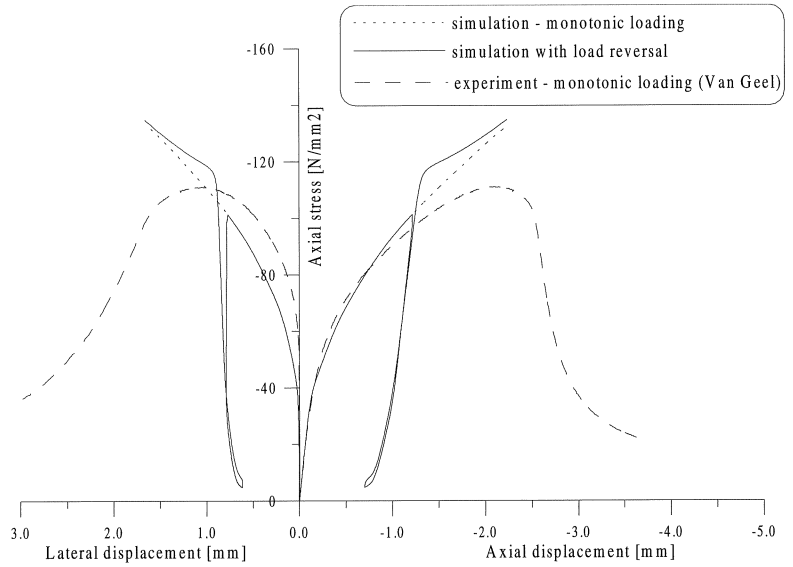

Fig. 22. Simulations of 10 % experiment with and without load reversal.

6.9 *Discussion of results*

With respect to the elastic branch in the loading diagram (stage I), it appears that the curves of the numerical simulation match quite well the experimental curves (figure 21). Comparison of the mechanical behaviour at stage II between simulation and experiment leads to more important differences. Especially the inelastic volumetric behaviour as displayed in the simulations differs considerably from the experiments. Although inelastic compactive behaviour is present, the lateral displacements in figure 21 are still too large.

To obtain the long hardening branch at stage II, a rather large amount of crushing is allowed (max. compaction is 50 %) in the simulations. This is more than it would be expected considering the properties of the bond zone discussed in section 1.1. This discrepancy can be explained from the three dimensional nature of the plane strain experiments at stage II. As the stresses in the out-of-plane direction find themselves in the region where crushing failure takes place, considerable inelastic compaction will take place in this direction. This effect is enlarged by the fact that the out-of-plane direction in the experiments is the casting direction (with higher bond zone porosity). This 3D-effect is not taken into account in the 2D analysis.

Not taking into consideration the 3D-effect may also account for the differences in lateral deformations between the experiments and simulations. However, considering the differences in the elastic stress distribution of the bond zone between the macrostress prescribed solution and the macrostrain prescribed solution for the RVE, application of the former instead of the latter solution may also explain these differences.

Though the unloading curve of figure 22 is very realistic, the reloading curve differs somewhat from those found in cyclic experiments (see figure 5). Due to the fact that the model does not allow any compressive force transfer between crack faces in an open crack, open bond cracks are immediately closed at reloading, resulting in a low initial reloading stiffness. Due to the irregular shape of the crack faces of tensile cracks in the bond zone, limited compressive force transfer through open cracks is likely to occur in the experiments, thus having a higher initial reloading stiffness as a consequence.

When the reloading curve of the simulation approaches the monotonic loading curve, the curve initially exceeds the monotonic loading curve. After a while the curves meet again (see figure 22). This phenomenon occurs due to a change in stress distribution in the individual bond zones during a load cycle. Due to considerable scattering of experimental results it is not quite clear whether this phenomenon also occurs in multiaxial cyclic compressive experiments.

Acknowledgement

This research is partly supported by the Dutch Technology Foundation (STW) under grant EBW22.2725.

References

BAZANT, Z.P., F.C. BISHOP & T.-P. CHANG (1986). Confined compression tests of cement paste and concrete up to 300 ksi. *ACI Journal* July-August: 553-560.

BONGERS, J.P.W. & H.J.G.M. VAN GEEL (1997). Numerical meso-scale simulations of multiaxially loaded concrete. In B.L. Karihaloo, Y.-W. Mai, M.I. Ripley & R.O. Ritchie (eds.), *Advances in Fracture Research* 2: 949-956. Amsterdam: Pergamon.

BONGERS, J.P.W. (1998). *2D Mesh generator for concrete composites.* Report TUE-BKO-98.18, Eindhoven University of Technology. The Netherlands.

BONGERS, J.P.W. (in prep.), Ph.D. Thesis, Eindhoven University of Technology. The Netherlands.

BOURDETTE, B., E. RINGOT & J.P. OLLIVIER (1995). Modelling of the transition zone porosity. *Cement and Concrete Research* 25/4: 741-751.

CHANG, C.S. (1993). Micromechanical modeling of deformation and failure for granulates with frictional contacts, *Mechanics of Materials* 16: 13-24

GEEL, H.J.G.M. van (1995). *Behaviour of concrete in plane strain compression.* Report TUE-BKO-95.19, Eindhoven University of Technology. The Netherlands.

GEEL, H.J.G.M. VAN & J.P.W. BONGERS (1997). Failure characteristics of concrete in plane strain compression. In B.L. Karihaloo, Y.-W. Mai, M.I. Ripley & R.O. Ritchie (eds.), *Advances in Fracture Research* 2: 965-972. Amsterdam: Pergamon.

GEEL, H.J.G.M. VAN (1998). *Concrete behaviour in multiaxial compression* – experimental research, Ph.D. Thesis, Eindhoven University of Technology. The Netherlands.

GOUDSWAARD, I. & R.A. VONK (1989). *A detection method for internal cracks in concrete specimens* (in Dutch). Report TUE-BKO-89.12, Eindhoven University of Technology. The Netherlands.

HILL, R. (1963). Elastic properties of reinforced solids: some theoretical principles, *Journal of the Mechanics and Physics of Solids* 11: 357-372

LARBI, J.A. (1991). *The cement paste-aggregate interfacial zone in concrete.* Ph.D. Thesis, Delft University of Technology. The Netherlands.

MIER, J.G.M. VAN (1984). *Strain-softening of concrete under multiaxial loading conditions.* Ph.D. Thesis, Eindhoven University of Technology. The Netherlands.

MIER, J.G.M. VAN (1992). Scaling in tensile and compressive fracture of concrete. In A. Carpinteri (ed.), *Applications of fracture mechanics to reinforced concrete*: 95-135. London: Elsevier.

ONCK, P., VAN DER GIESSEN, E. (1997). Microstructurally-based modelling of intergranular creep fracture using grain elements, *Mechanics of Materials* 26: 109-126

SLATE, F.O. & K.C. HOVER (1984). Microcracking in concrete. In A. Carpinteri & A.R. Ingraffea (eds.), *Fracture Mechanics of Concrete*: 137-159. The Hague: Martinus Nijhoff Publishers.

SMIT, R.J.M. (1993). *Toughness of heterogeneous polymeric systems - a modeling approach*, Ph.D. Thesis, Eindhoven University of Technology, The Netherlands.

STROEVEN, P. (1973). *Some aspects of the micro-mechanics of concrete*. Ph.D. Thesis, Delft University of Technology. The Netherlands.

VONK, R.A. (1992). *Softening of concrete loaded in compression*, Ph.D. Thesis, Eindhoven University of Technology. The Netherlands.

WITTMANN, F.H. (1987). Structure of concrete and crack formation. In K.P. Herrmann & L.H. Larsson (eds.), *Fracture of Non-Metallic Materials*: 309-340. Dordrecht: Reidel.